Design guideline for PCB integrated, high bandwidth, current slope sensing based on a planar Rogowski coil

Johannes Stoß, Christoph Wurster, Nikolas Menger, Matthias Brodatzki, Andreas Liske, Marc Hiller
Karlsruhe Institute of Technology (KIT)
Engelbert-Arnold-Straße 5
76131 Karlsruhe, Germany
Tel.: +49 / (0) 721 608 - 41647
Fax: +49 / (0) 721 608 - 358854
E-Mail: johannes.stoss@kit.edu
URL: www.eti.kit.edu

Keywords

«Current derivative», «Current sensor», «Non-linear control», «Estimation technique»

Abstract

This paper shows the design process of a planar Rogowski coil integrated in the Printed-Circuit-Board (PCB) for direct current slope measurement. Focus lies on the analytic estimation of the coil parameters with respect to specific limitations and the analog signal processing for a simplified design process. All analytic derivations are verified by measurements.

Introduction

Adaptive control of electrical machines and online parameter identification usually rely on the usage of test signals to evaluate the system parameters at the current operating point. In recent years, new methods have been proposed that use the PWM excited current slopes of the inverter instead of additional test signals [1–3].

To measure the current slope, one possible solution is the derivation of the measured current signal using a least squares algorithm [4]. This requires high bandwidth current sensors, fast and precise Analog-Digital-Converters (ADC) and intense signal processing for stable calculation of the derivative and filtering. Specialized Field Programmable Gate Array (FPGA) implementation reduces hardware resources significantly and minimizes calculation time to one FPGA cycle [4].

A different approach is the usage of a dedicated current derivative sensor based on a Rogowski coil [5]. Different designs for dedicated PCB sensors have been published either to extend bandwidth or as cheaper alternative to a conventional current sensor [6, 7].

This paper describes the design process of a PCB integrated planar Rogowski coil using an analytical model. Validation is done over a variety of parameters with a dedicated PCB design of seven different planar Rogowski coils. Furthermore, a typical application based on a three-phase two-level inverter is outlined.

Analytical evaluation of the coil parameters

The Rogowski coil is implemented as a built-in structure in a four-layer PCB (optional six-layer if shielding is required). This reduces parameter variation due to manufacturing tolerances compared to a two layer approach proposed in [6]. Since most modern PCB layouts require more than two layers, the sensor can be implemented with minimal additional effort.

The analytical estimation of the sensor parameters allows to fit the design to specific requirements and limitations like maximum space, required output voltage, current gradients, layer stack, minimum distance between vias etc. The analytical model allows to calculate the gain and bandwidth of the Rogowski coil by analytical calculation of the equivalent circuit parameters (Fig. 5 – yellow) only based on the geometric shape.

The planar Rogowski coil can be described as a coreless transformer with rectangular shape (Fig. 1). The primary side represents the load path while the secondary side is the Rogowski coil. Therefore, the

self-inductance and capacitance, the mutual inductance and the coupling capacitance of the equivalent circuit of the transformer are analytically calculated using concentrated elements. This approach is valid below the first resonance frequency [8].

In [9] the self-inductance L_{xx} of a rectangular coil is described. Using the geometric parameters given in Fig. 1b) the self-inductance of the Rogowski coil can be calculated. Whereas N_x is the number of windings, b the width, l the length and h the height of the coil using $g = \sqrt{b^2 + h^2}$.

$$
\begin{aligned}
L_{\mathrm{xx}} = {}& 2 \cdot \frac{\mu_0}{\pi} \cdot N_x{}^2 \cdot \frac{h \cdot b}{l} \\
& \left[\frac{l}{2 \cdot b} \cdot asinh\left(\frac{h}{l}\right) + \frac{l}{2 \cdot h} \cdot asinh\left(\frac{b}{l}\right) - \left(1 - \frac{b^2}{l^2}\right) \cdot \frac{l}{2b} \right. \\
& \cdot asinh\left(\frac{h}{l \cdot \sqrt{\left(1 + \frac{b^2}{l^2}\right)}}\right) - \left(1 - \frac{h^2}{l^2}\right) \cdot \frac{l}{2h} \cdot asinh\left(\frac{b}{l \cdot \sqrt{\left(1 + \frac{h^2}{l^2}\right)}}\right) - \frac{b}{2l} \\
& \cdot asinh\left(\frac{h}{b}\right) - \frac{h}{2l} \cdot asinh\left(\frac{b}{h}\right) \cdot \left(h \cdot \frac{b}{l^2 \cdot \sqrt{\left(1 + \frac{g^2}{l^2}\right)}}\right) + \frac{l^2}{3 \cdot h \cdot b} \\
& \cdot \sqrt{\left(1 + \frac{g^2}{l^2}\right)} \cdot \left(1 - \frac{g^2}{2 \cdot l^2}\right) + \frac{l^2}{3 \cdot h \cdot b} - \frac{l^2}{3 \cdot h \cdot b} \cdot \sqrt{1 + \frac{h^2}{l^2}} \cdot \left(1 - \frac{h^2}{2 \cdot l^2}\right) \\
& \left. - \frac{l^2}{3 \cdot h \cdot b} \cdot \sqrt{1 + \frac{b^2}{l^2}} \cdot \left(1 - \frac{b^2}{2 \cdot l^2}\right) + \frac{l}{6 \cdot h \cdot b} \cdot \frac{g^3 - h^3 - b^3}{l^2} \right]
\end{aligned}
\tag{1}
$$

To improve calculation accuracy, deviations based on the wire geometry can be reduced using the analytic approximations of Grover and Rosa [10, 11].

Furthermore the via inductance can be corrected using [12].The mutual inductance (M) is calculated using Faraday's law of induction with the geometric parameters given in Fig 1, based on a round wire estimation. The induced voltage on a parallel rectangular loop with the height h and width b in distance d to an ideal wire can be calculated to:

$$
V_{\mathrm{ind}} = \frac{d\Psi}{dt} = \int \frac{d\vec{B}}{dt} \cdot d\vec{A} = \mu_0 \frac{b}{2\pi} \cdot \frac{di}{dt} \int_d^{h_2+d} \frac{1}{r} \cdot dr = \mu_0 \frac{b}{2\pi} \cdot \ln\left(\frac{h_2 + d}{d}\right) \cdot \frac{di}{dt}
\tag{2}
$$

To calculate the induced voltage on each loop of the Rogowski coil, the primary side windings are distributed to an infinite number of small ideal round wires. This model is applied to approximate the average distance of all ideal wires on the primary side to the center of the Rogowski coil using the hardware parameters N_X as the winding numbers, w_X the linewidth and l_X the length of the primary side (index 1) and the Rogowski coil (index 2):

$$
d_1 = (l_1 - N_1 \cdot w_1/2)/2 + r_0
\tag{3}
$$

It is assumed that both coils are perfectly centered. Adding the average distance from each winding of the Rogowski coil to its center, the average distance d is calculated to:

$$
d = d_1 + \frac{l_2}{4} = \frac{l_2}{4} + \frac{\left(l_1 - N_1 \cdot \frac{w_1}{2}\right)}{2} + r_0
\tag{4}
$$

Doubling the induced voltage to take the bottom layer windings into account and scaling it with the winding numbers of each side, the induced voltage is calculated to:

$$V_{\text{ind}} = 2 \cdot \mu_0 \cdot N_1 \cdot N_2 \cdot \frac{b}{2\pi} \cdot \ln\left(\frac{h_2}{d} + 1\right) \cdot \frac{di_2}{dt} \tag{5}$$

To calculate the mutual inductance, the primary side parasitic elements are neglected since their influence on the sensor characteristics is typically small. This gives the ideal induced voltage:

$$V_{\text{ind}} = M_1 \cdot \frac{di_2}{dt} = M_1 \cdot \frac{N_2}{N_1} \cdot \frac{di_1}{dt} = M_2 \cdot \frac{di_1}{dt} \tag{6}$$

Using 6 and 7 the mutual inductance of the sensor can be calculated.

$$M_2 = 2\frac{\mu_0 \cdot N_2^2 \cdot b}{2\pi} \cdot \ln\left(\frac{h}{\frac{l_2}{4} + \frac{\left(l_1 - N_1 \cdot \frac{w_1}{2}\right)}{2} + r_0} + 1\right) \tag{7}$$

With the inductance L_{xx} and the mutual inductance, the stray inductance can be calculated:

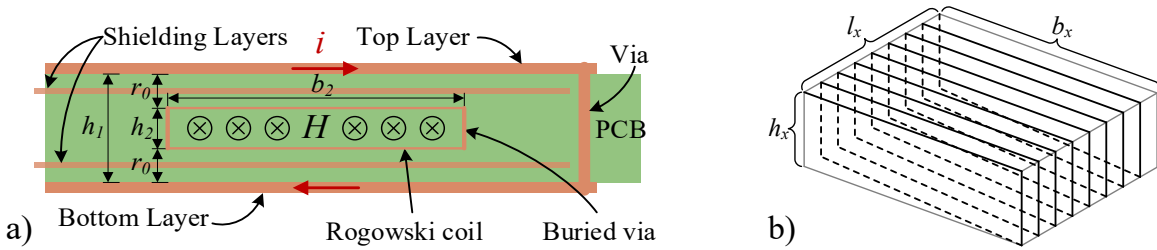$$L_{\sigma,\text{x}} = L_{\text{xx}} - M \tag{8}$$

Fig. 1: Dimensions of the Rogowski coil and primary winding.

In addition to the inductances the self- and coupling capacitance needs to be estimated. The coupling capacitance from the load path to the Rogowski coil is analyzed using the estimation for asymmetric striplines given in [13].

Therefore, it is assumed that the linewidth of the load path is significantly larger than the linewidth of the Rogowski coil. With the length of the stripline approximated to $2 \cdot N_2 \cdot b$ and the linewidth w the capacitance is calculated.

$$C_{\text{C}} = 2 \cdot N_2 \cdot b \cdot \epsilon_0 \cdot \epsilon_r$$

$$\cdot \left[\left(\frac{w}{r_0} + \frac{w}{r_0 + h}\right)^n + \left(2 \cdot pi\left(\frac{1}{ln\left(8 \cdot \frac{h + 2r_0}{pi \cdot w} + 1\right)} - \frac{pi \cdot w}{8 \cdot (h + 2r_0)}\right)\right)^n\right]^{\frac{1}{n}} \tag{9}$$

$$n = 1.39 + \left(\frac{r_0}{h + 2r_0} - 0.83\right) \cdot \left(0.44 + 0.46 \cdot e^{-\frac{w}{0.3(h+2r_0)}}\right) \tag{10}$$

The self-capacitance of the Rogowski coil is approximated in two steps. First, the biplanar capacitance of each line to the next on a different layer is estimated using the formulas of the ideal plate capacitor. The surface area is assessed to $A_{\text{c,xy}} = \frac{w^2 \cdot b}{2p}$ with the pitch $p = l_2/N_2$.

$$C_{\text{xy}} = \epsilon_0 \cdot \epsilon_r \frac{w^2 \cdot b}{2p \cdot h} \tag{11}$$

The coplanar capacitance of each line to the next on the same layer is calculated according to [14]. For $\frac{1}{\sqrt{2}} < \left(\frac{p}{p+2w}\right)$ and using c_0 as the speed of light, the coplanar capacitance is:

$$C_{xx} = \frac{\epsilon_0 \cdot \epsilon_r \cdot w \cdot b}{120 \cdot c_0 \ln\left(-\dfrac{2}{\sqrt{\frac{p}{p+2w}}-1}\left(\sqrt{\frac{p}{p+2w}}+1\right)\right)} \tag{12}$$

The overall capacitance of each side is given by the sum of all partial capacitances:

$$C_{\sigma,x} = (2 \cdot N_x - 1) \cdot C_{xy} + (N - 1) \cdot C_{xx} \tag{13}$$

The dc resistance of each side is calculated using d as the layer thickness and ρ_{cu} as specific resistance of copper:

$$R_{cu,x} = \frac{2 \cdot N_x \cdot b \cdot \rho_{cu}}{d \cdot w} \tag{14}$$

For higher frequency operation, the resistance will increase due to skin effect. The higher coil resistance leads to a gain reduction of the sensor as shown in 15. To improve the high frequency model accuracy, the influence of the skin effect can be calculated using the research of Haefner and Cockcroft [15, 16]. Furthermore, via impedance can be added to the calculations [12].

The transfer function G of the sensor under neglection of the parasitic elements on the primary side and the coupling capacitance is given in [8]. It was adapted to the purpose of di/dt measurement and transferred to elements on the output side of the transformer.

$$G = \frac{V_{out}}{di_1/dt} = \frac{\frac{N_1}{N_2} \cdot M}{L_{\sigma,2} \cdot C_{\sigma,2} \cdot \left(\frac{N_2}{N_1}\right)^2 \cdot s^2 + \left(R_{cu,2} \cdot C_{\sigma,2} + \frac{L_{\sigma,2}}{R_d}\right) \cdot \frac{N_2}{N_1} \cdot s + 1 + \frac{R_{cu,2}}{R_d}} \tag{15}$$

According to [17] the resonance frequency can be estimated to:

$$f_{res,cm} = \frac{1}{2\pi \sqrt{L_{\sigma,2} \cdot C_{\sigma,2}}} \sqrt{\frac{R_{cu,2} + R_d}{R_d}} \tag{16}$$

According to [8] the ideal damping resistance is calculated using the parasitic inductance and capacitance of the Rogowski coil, neglecting the coil resistance.

$$R_{d,DM} = \frac{1}{2}\sqrt{L_{\sigma,2}/C_{\sigma,2}} \tag{17}$$

The common mode transfer function of the unshielded Rogowski coil with one connection tied to ground can be derived from the circuit diagram in fig. 5.

$$\frac{V_{out}}{V_{CM}} = \frac{\frac{(M + L_{\sigma,2})C_c}{2}s^2 + \frac{R_{cu,2}C_c}{2}s}{(M + L_{\sigma,2})\left(\frac{C_c}{2} + C_{\sigma,2}\right)s^2 + \left(R_{cu,2}C_{\sigma,2} + R_{cu,2}\frac{C_c}{2} + \frac{(M + L_{\sigma,2})}{R_d}\right)s + \frac{R_{cu,2} + R_d}{R_d}} \tag{18}$$

The resonance frequency caused by capacitive coupling, parasitic and mutual inductance can be derived from equation 17 and [17]:

$$f_{\text{res,cm}} = \frac{1}{2\pi \sqrt{(M + L_{\sigma,2})\left(\frac{C_c}{2} + C_{\sigma,2}\right)}} \sqrt{\frac{R_{\text{cu2}} + R_d}{R_d}} \tag{19}$$

Using the estimations of [8] the damping resistance for common mode coupling can be calculated to:

$$R_{\text{d,CM}} = \frac{1}{2} \sqrt{\frac{M + L_{\sigma,2}}{\left(\frac{C_c}{2} + C_{\sigma,2}\right)}} \tag{20}$$

The damping resistance can be chosen according to the expected dv/dt of the application within the range of $R_{\text{d,CM}}$ and $R_{\text{d,DM}}$. High dv/dt may require further diminution of R_d, which will lead to reduced sensor bandwidth and output voltage and should therefore be chosen with care.

Verification of the analytical model

Fig. 2.: a) PCB with Designs 5-7. Load path colored red, Rogowski coil blue. b) Frequency response of Designs 5-7.

To verify the analytical model, two dedicated PCBs (second PCB shown in fig. 2 a) were constructed, offering seven different designs of the planar Rogowski coil with identical surface area. The design parameters are given in Table I. Design 2 is chosen identical to Design 1 but features two additional shielding layers to reduce common mode disturbances. Effects of shielding will be discussed in the next chapter. The impedance of the planar Rogowski coil designs were measured with *Keysight E4980AL-102* 1 MHz LCR meter. The impedance was then fitted to the equivalent circuit using Matlab® Zfit [18].

Table I: Parameters of the sensors. All length specifications in mm

	Design 1	Design 2	Design 3	Design 4	Design 5	Design 6	Design 7	inverter
N_1	2	2	1	2	2	2	2	2
l_1	45.4	45.4	45.4	45.4	45.4	45.4	45.4	45.4
b_1	64.5	64.5	64.5	64.5	64.5	64.5	64.5	65.5
h_1	2.06	2.06	2.06	2.06	2.06	2.06	2.06	1.9
w_1	22.6	22.6	45.4	22.6	22.6	11.3	22.6	22.8
d_1	0.09	0.09	0.09	0.09	0.09	0.09	0.09	0.07
N_2	50	50	50	50	50	50	50	50
l_2	36.75	36.75	36.75	45	36.75	36.75	36.75	36.75
b_2	40	40	40	40	40	40	20	40
h_2	1.37	1.37	1.37	1.37	1.37	1.37	1.69	1.5
w_2	0.2	0.2	0.2	0.2	0.55	0.2	0.2	0.2
d_2	0.06	0.06	0.06	0.06	0.06	0.06	0.06	0.07

Table II: Estimation errors. Positive values indicate smaller measurements than expected.

	Design 1	Design 2	Design 3	Design 4	Design 5	Design 6	Design 7
M_2	3.9%	4.2%	5.1%	-3.8%	3.7%	2.6%	-17.6%
R_{cu2}	-7.6%	-5.1%	-1.9%	-3.9%	-5.07%	-1.9%	7.2%
$C_{\sigma 2}$	1.5%	-77%	1.8%	50%	24.9%	22.9%	-74%
$L_{\sigma 2}$	-44%	-28%	-46%	-78%	19%	-30%	36%
C_C	7.7%	not estimated	8.4%	-0.4%	42%	2.6%	-28%

Table II shows the deviation of the estimation presented in the first chapter to the measured results. Due to large measurement uncertainty and the negligible influence on the sensor characteristics, the measurements of the load path are not displayed. Deviations between the calculations and measurements of the Rogowski coil may have several reasons:

The parameter estimations only consider the sensor traces and therefore the impedance of the connections to the measurement terminals are neglected in the calculations. Furthermore, the actual track width of the PCB can vary by up to 20 % and layer thickness up to 15 % the due to the manufacturing process [19]. Calibration of the designed track width to the manufactured PCB can be achieved by the R_{DC} evaluation, therefore the trackwidth was corrected by -17 % in design 1-6 which share the same layers. Since the Rogowski coil in design 7 is placed on different layers, no correction was applied.

The impedance fit of Matlab® Zfit uses the reduced circuit with concentrated elements shown in fig. 5 with neglection of skin and proximity effect. This improves the robustness of the solution but leads to lower measurement accuracy. Even with partial uncertainty of the design parameters and measurement tolerances, the estimations show a sufficient agreement to the measurements.

Evaluation of the sensor characteristics and the mutual inductance is performed by a frequency response analysis up to 20 MHz with the *Keysight MSOX3024T* oscilloscope using a $1\ \Omega\ \pm 1\ \%$ shunt resistor for input current measurement and $R_d = 82\ \Omega\ \pm 1\ \%$. One output of the Rogowski coil is connected to ground. The input current was generated using the built-in signal-generator. Fig. 3 a) confirms the analytical model for the common mode frequency response by comparison with the measured frequency response. The measurements were performed with one input of the load path connected to the signal-generator while the second input was left open. Since one output of the Rogowski coil is connected to ground, common mode disturbance can couple trough $C_C/2$ as shown in equation 18.
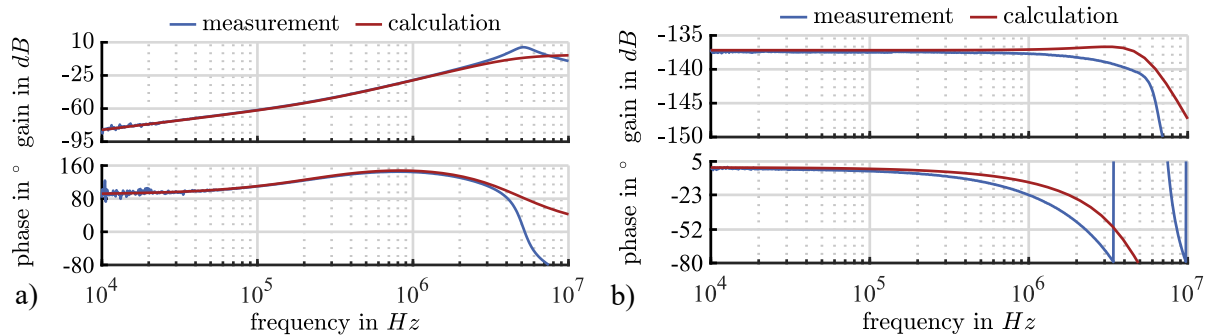

Fig. 3: Comparison of measured to analytical estimated frequency response a) common mode frequency response (equation 19) b) differential mode frequency response (equ.16)

Fig. 3 b) shows the measured frequency response analysis compared to the analytically calculated frequency response between 1 kHz and 10 MHz of design 1. The results show sufficient agreement of the estimation below the first resonance frequency. As changes in wire geometry are not covered by the presented calculations, larger deviations are expected in design 5 as it features increased linewidth. In summary, the measurements show that the system behavior can be sufficiently approximated by the presented analytical approximations.

Reduction of common mode distortion

Common mode distortions are mainly induced through capacitive coupling by the large surface areas and low distance of the primary and secondary windings. Reduction can be achieved by reducing the common surface areas of the Rogowski coil and the load path, additional shielding, filtering of the output signal, or a differential Rogowski coil design as proposed in [20].

A possible filter design using y-capacitors is shown in fig. 5. It reduces the common mode disturbances due to the capacitive voltage divider by the y-capacitors and the coupling capacitance. Therefore, the capacitors are chosen significantly larger than the coupling capacitance. It should be noted, that adding output capacitors will have a similar effect as increasing $C_{\sigma,2}$, which results in reduction of the sensor bandwidth.

Effects of the reduction of the common surface area are explored in Design 6 shown in fig. 2 a). The load path is placed on the edges of the Rogowski coil, resulting in 22 % reduced output voltage compared to design 1. The Rogowski coil was placed on layer 2 and 5 resulting in 23 % increased height while also reducing the space between load path and Rogowski coil by 60 %. The smaller cross section area on the load path reduces the maximum current of the design but also reduces common mode capacitance by 58 % compared to design 1 even with smaller distance. This results in smaller filter capacitors or higher damping resistor and therefore increased bandwidth.

In Design 2 an additional ground layer was added between top/bottom-layer and the Rogowski coil. Compared to Design 1 the shielding reduces the common mode capacitance by a factor of 257 (1.35 pF – design 2 vs. 349 pF – design 1). Fig. 4 a) shows the resulting equivalent circuit diagram. The connection of the ground plane adds an additional parasitic inductance to ground, which can lead to additional resonance if the connection is not designed properly. The effects of high $L_{\sigma,\mathrm{GND}}$ are shown by measurements in Fig. 4 b). To reduce current spikes on the ground connection, the shielding can be connected to the dc-link potentials of the inverter as well. This may require additional filtering of the dc-link common mode voltage by y-capacitors.
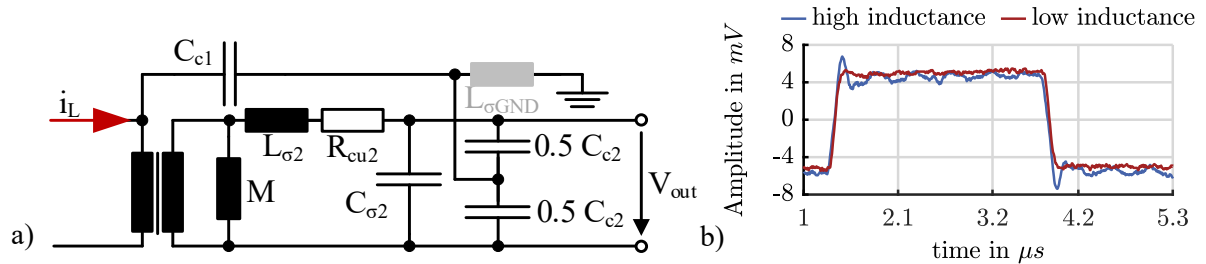

Fig. 4: Reduced equivalent circuit diagram of the Rogowski coil with ground connection (left). Measurements with high and low inductance to ground (right).

Design considerations and limitations

The analytical model shows that different compromises need to be made during the design process. The mutual inductance should be maximized with respect to the physical limitations to offer a good signal to noise ratio (SNR) $\left(U = -L\frac{\mathrm{d}i}{\mathrm{d}t}\right)$. Therefore, the linewidth of the load path should be chosen as small as possible to increase the flux linkage in the Rogowski coil.

To increase the output voltage, the cross section of the coil can be enlarged. This also leads to an increased coupling capacitance and therefore greater common mode distortion and bandwidth reduction. The distortion can be filtered by y-capacitors, which will decrease the bandwidth of the designed coil or reduced by a differential coil design [20]. For this reason, the cross-sectional area should only be increased to such an extent that the desired bandwidth can still be achieved.

Shielding of the planar Rogowski coil lowers common mode disturbances more effective than filtering with only slightly decreasing the bandwidth. Focus should be a low parasitic inductance of the shielding connection to reduce disturbances induced by the parasitic resonant circuit of the coupling capacitance and shielding connection. Furthermore, shielding requires two additional layers making it less cost efficient.

Another way to increase the output voltage is the maximation of the winding numbers on each coil. Usually, the number of windings of the Rogowski coil is limited by the available space on the PCB and

the minimum clearance of the traces and vias defined by the manufacturer. The number of windings on the primary side is basically limited by the required cross-section area for the designed output current. Increasement of windings raises the output voltage but also increases $C_{\sigma x}$ and C_c due to larger surface areas. This will require additional damping by decreasing R_d which leads to reduced bandwidth and output voltage. To increase the bandwidth an additional characteristic shaper proposed in [21] can be implemented.

Typical Application

Fig. 6 a) shows an inverter design including three-phase current-, current slope- and voltage-sensors, as well as a DC-link voltage-sensor to support current slope-based machine control and parameter identification algorithms. The inverter is designed to support switching frequencies up to 100 kHz, DC-link voltages up to 60 V and phase RMS currents up to 25 A. The design parameters of the planar Rogowski coil on the inverter given in table II. Compared to design 1-7, this design has higher common mode coupling due to smaller distance between the Rogowski coil and the load path requiring higher filter effort.

The signal processing is done by a *Xilinx Zynq-7030* System on Chip (SoC) using a 16bit, 5 MS/s (mega samples per second) *LTC2325 ADC* with additional active input voltage divider.

Analog signal processing

The Rogowski coil is evaluated by an analog circuit to adjust voltage levels, reduce noise and damp the coil (Fig. 5). The resistor R_d is iteratively chosen to 11.2 Ω to provide a sufficient output voltage and damping of the circuit. Furthermore, the passive voltage divider defines the potential of the Rogowski coil.

In the designed inverter shown in Fig. 6 the Rogowski coil is placed next to each half bridge which leads to high voltage gradients during switching and therefore a high common mode distortion due to the coupling capacitance C_C. To reduce the common mode noise C_{LP1} is chosen to $10 \cdot C_C$.

R_{LP1} is selected to have an additional differential lowpass with the edge frequency set to the Nyquist frequency of the ADC. Since R_{LP1} reduces the output voltage of the sensor, the resistance should be chosen small compared to R_d.

$$R_{LP1} = \frac{1}{2\pi f \cdot C_{LP1}} \tag{21}$$

When controlling highly utilized electrical machines, the current slope needs to be measured precisely under changing inductances. The operational amplifier AD850ARMZ allows to change the gain with two additional IOs in four steps to 1, 2, 5 and 10. This allows to set a higher gain in high inductance operating points and decrease the gain when saturation or anisotropic behavior in the electrical machine leads to decreased inductances.
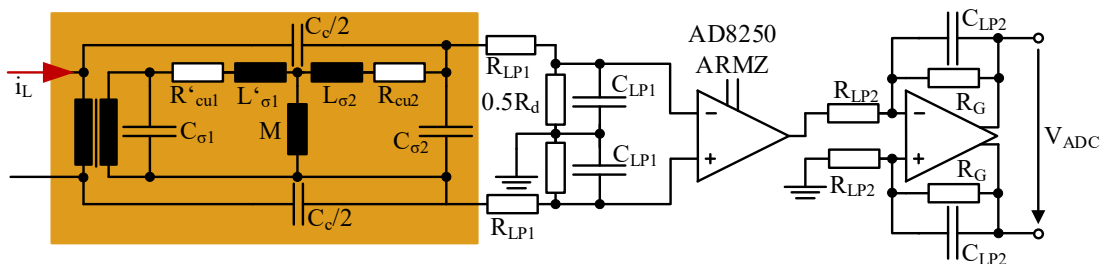

Fig. 5: equivalent circuit diagram of the Rogowski coil (yellow) and analog signal processing.

Usually, the ADC is located next to the control unit while the measurement is preformed next to the powerpath. For a more robust signal transmission the voltage levels are increased by the second operational amplifier to the ±10 V input voltage level of the ADC. In addition, the transmission is changed from single-ended to a differential signal. C_{LP2} is chosen depending on R_{LP2} to set the cutoff frequency of the second lowpass the to the Nyquist frequency of the ADC to provide additional filtering and reduce oscillations during transient signal changes.

$$C_{LP2} = \frac{1}{2\pi f \cdot R_{LP2}} \tag{22}$$

Testbench measurements

The designed inverter was validated using a back-to-back motor testbench with two Nanotec DB59C024035R PMSMs. The inverter was operated at 20 kHz PWM frequency and 15 V DC-Link Voltage. The static gain of the second operational amplifier was set to 10. All lowpass filter were designed with an edge frequency of 2.5 MHz. The variable Gain at AD8250ARMZ was set to the maximum of 10 to show the performance under maximum noise level.

Table III: Nominal values of the inverter (left) Operating point (middle) and Machine Parameters of Nanotec DB59C024035R (right)

Nominal values		Operating Point - inverter		Operating point - machine	
PWM Frequency	100 kHz	PWM Frequency	20 kHz	R_s	0.135 Ω
DC-Link Voltage	60 V	DC-Link Voltage	15 V	L_d	0.2 mH
Max. Power	1.4 kW	Rotational speed	800 rpm	L_q	0.2 mH
RMS Phase Current	25 A	RMS Phase Current	0.5 A	Ψ_{pm}	11.7 mVs

The measurement shown in Fig. 6 was performed under the conditions of Table III. The di/dt reference signal (fig. 6 b) – red) was measured by a 50 MHz *Tectronix A6302* current probe and processed in MATLAB using a 100th order differential filter with an edge frequency of 2.5 MHz and compensated group delay.

The measurements of the ADC values of the Rogowski coil and the current probe were synchronized by an external trigger signal connected to the SoC and the oscilloscope.
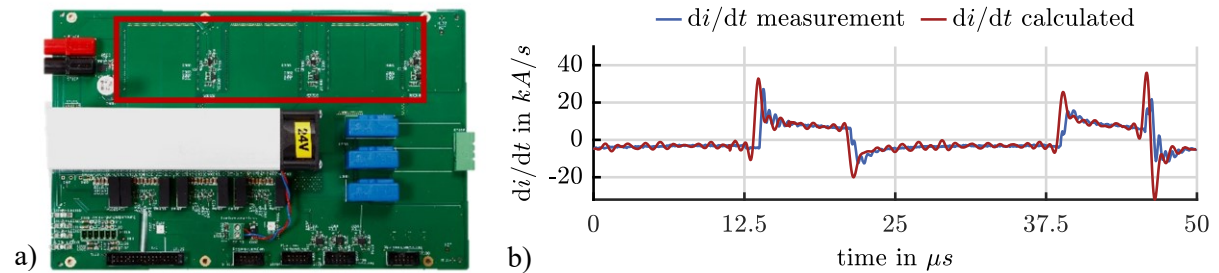

Fig. 6: a) Designed inverter prototype including planar Rogowski coils (red). b) Comparison of a measured current with a phase delay compensated derivative filter (red) and the planar Rogowski coil (blue) on a Nanotec DB59C024035R.

Compared to the postprocessed current measurements the direct current slope measurement of the planar Rogowski coil tends to have lower noise level. The additional propagation delay due to the analog signal processing delay is 300 ns. The oscillations after each switching event depend on the parasitic capacitances and inductances of the test bench and cables. In the performed measurement the di/dt values were stable after 2.25 µs.

Conclusion

This paper shows the design process of a di/dt sensor by a planar Rogowski coil. The sensor parameters were analytically estimated to allow a simplified design process for customized sensors with respect to the individual requirements and limitations of each application. The analytical evaluation was afterwards verified by different measurements and impact of common mode coupling was discussed. Furthermore, a low voltage two-level drive inverter was designed to prove the performance under real operating conditions of the sensor. In addition, the analog signal processing of the planar Rogowski coils in the inverter was described. As outlined in the paper, common mode reduction is crucial to the design as it has significant influence on the sensor performance. Therefore, the load track with should be adapted to each application to reduce the coupling capacitance C_C and increase the mutual inductance M.

References

[1] S. Decker, J. Stoss, A. Liske, M. Brodatzki, J. Kolb, and M. Braun, "Online Parameter Identification of Permanent Magnet Synchronous Machines with Nonlinear Magnetics based on the Inverter Induced Current Slopes and the dq-System Equations," in *2019 21st European Conference on Power Electronics and Applications (EPE '19 ECCE Europe)*, Genova, Italy, 2019, P.1-P.10.

[2] A. Liske and M. Braun, "Direct adaptive current control in space vector overmodulation mode," in *2017 IEEE 12th International Conference on Power Electronics and Drive Systems (IEEE PEDS 2017): Hawaii Convention Center, Honolulu, Hawaii, USA, 12-15 December 2017*, Honolulu, HI, 2017, pp. 715–720.

[3] M. Schroedl, "Operation of the permanent magnet synchronous machine without a mechanical sensor," in *1990 Fourth International Conference on Power Electronics and Variable-Speed Drives (Conf. Publ. No. 324)*, 1990, pp. 51–56.

[4] A. Liske, S. Decker, and M. Braun, "Resource optimal FPGA implementation of a Least-Squares-Estimator for fast and robust online measurement of current slope and absolute value," in *2019 21st European Conference on Power Electronics and Applications (EPE '19 ECCE Europe)*, Genova, Italy, 2019, pp. 1–10.

[5] S. Decker, A. Liske, D. Schweiker, J. Kolb, and M. Braun, "Measurement of Two-Level Inverter Induced Current Slopes at High Switching Frequencies for Control and Identification Algorithms of Electrical Machines," in *Power electronics for sustainable society: The 2018 International Power Electronics Conference - ECCE Asia : IPEC 2018 - ECCE Asia Niigata : May 20-24, 2018, Toki Messe Niigata Convention Center*, Niigata, 2018, pp. 2848–2853.

[6] L. Zhao, J. D. van Wyk, and W. G. Odendaal, "Planar embedded pick-up coil sensor for integrated power electronic modules," in *APEC 2004: Nineteenth Annual IEEE Applied Power Electronics Conference and Exposition ; 22 - 26 February 2004, the Disneyland Hotel, Anaheim, California*, Anaheim, CA, USA, 2004, pp. 945–951.

[7] B. Parkhideh and S. J. Nibir, "Hybrid Magnetoresistor-Planar Rogowski Current Sensing Scheme With Folded Trace Magnetic Field Concentration Technique," *IEEE Sensors Journal*, vol. 17, no. 11, pp. 3446–3452, 2017, doi: 10.1109/JSEN.2017.2691262.

[8] T. Guillod, D. Gerber, J. Biela, and A. Muesing, "Design of a PCB Rogowski Coil based on the PEEC Method," in *2012 7th International Conference on Integrated Power Electronics Systems (CIPS)*, 2012, pp. 1–6.

[9] Y. Niwa, *A Study of Coils Wound on Rectangular Frames with Special Reference to the Calculation of Inductances*: Electrotechnical Laboratory, 1924. [Online]. Available: https://books.google.de/books?id=2cncHAAACAAJ

[10] E. B. Rosa, "Calculation of the self-inductance of single-layer coils,"

[11] F. W. Grover, "A comparison of the formulas for the calculation of the inductance of coils and spirals wound with wire of large cross section," 1929.

[12] M. E. Goldfarb and R. A. Pucel, "Modeling via hole grounds in microstrip," *IEEE Microw. Guid. Wave Lett.*, vol. 1, no. 6, pp. 135–137, 1991, doi: 10.1109/75.91090.

[13] W. Tang and B. Jiang, "CAD formula of asymmetric stripline via synthetic asymptote," *Microw. Opt. Technol. Lett.*, vol. 47, no. 2, pp. 143–145, 2005, doi: 10.1002/mop.21105.

[14] C. R. Paul, *Analysis of multiconductor transmission lines*. Hoboken, New Jersey, Piscataway, New Jersey: Wiley-Interscience IEEE Press; IEEE Xplore, 2007.

[15] J. D. Cockcroft, "Skin Effect in Rectangular Conductors at High Frequencies," *Proceedings of the Royal Society of London. Series A, Containing Papers of a Mathematical and Physical Character*, vol. 122, no. 790, pp. 533–542, 1929. [Online]. Available: http://www.jstor.org/stable/95158

[16] S. J. Haefner, "Alternating-Current Resistance of Rectangular Conductors," *Proc. IRE*, vol. 25, no. 4, pp. 434–447, 1937, doi: 10.1109/JRPROC.1937.229047.

[17] Y. Wang, J. Li, Y. Hu, R. An, Z. Cai, and R. He, "Analysis on the Transfer Characteristics of Rogowski-coil Current Transformer and Its Influence on Protective Relaying," *EPE*, vol. 05, no. 04, pp. 1324–1329, 2013, doi: 10.4236/epe.2013.54B251.

[18] Jean-Luc Dellis, *Zfit*. [Online]. Available: https://de.mathworks.com/matlabcentral/fileexchange/19460-zfit (accessed: May 30 2021).

[19] Multi-CB company group, *Manufacturing tolerances*. [Online]. Available: https://www.multi-circuit-boards.eu/en/quality/manufacturing-tolerances.html (accessed: Jun. 24 2021).

[20] Jan Niklas Fritz, Christoph Neeb, and Rik W. De Doncker, "A PCB Integrated Differential Rogowski Coil for Non-Intrusive Current Measurement Featuring High Bandwidth and dv/dt Immunity,"

[21] H. Li, Z. Xin, X. Li, J. Chen, P. C. Loh, and F. Blaabjerg, "Extended Wide-Bandwidth Rogowski Current Sensor With PCB Coil and Electronic Characteristic Shaper," *IEEE Trans. Power Electron.*, vol. 36, no. 1, pp. 29–33, 2021, doi: 10.1109/TPEL.2020.3001058.